Title

Realization of Electron Antidoping by Modulating the Breathing Distortion in BaBiO3

Journal

Nano Letters, 21(9)

ISSN

1530-6984

Authors

Cao, Hui

Guo, Hongli

Shao, Yu-Cheng

et al.

Publication Date

2021-05-12

DOI

10.1021/acs.nanolett.1c00750

Peer reviewed

Realization of electron antidoping by modulating the breathing distortion in $BaBiO_3$

Hui Cao[#], Hongli Guo[#], Yu-Cheng Shao, Qixin Liu, Xuefei Feng, Qinwen Lu, Zhongping Wang, Aidi Zhao, Atsushi Fujimori, Yi-De Chuang, Hua Zhou[*], and Xiaofang Zhai[*]

Dr. Hui Cao, Dr. Hongli Guo, Qixin Liu, Qinwen Lu, Prof. Zhongping Wang
Department of Chemical Physics, Department of Physics, Physics Experiment Teaching Center, and Hefei National Laboratory for Physical Sciences at the Microscale, University of Science and Technology of China, Hefei 230026, China

Prof. Aidi Zhao, Prof. Xiaofang Zhai
School of Physical Science and Technology, ShanghaiTech University, Shanghai 201210, China
E-mail: zhaixf@shanghaitech.edu.cn

Dr. Hui Cao, Dr. Hua Zhou
X-ray Science Division, Advanced Photon Source, Argonne National Laboratory, Lemont, IL 60439, USA
E-mail: hzhou@anl.gov

Dr. Hongli Guo
School of Physics and Technology and Key Laboratory of Artificial Micro- and Nano-Structures of Ministry of Education, Wuhan University, Wuhan 430072, China

Dr. Yu-Cheng Shao, Dr. Xuefei Feng, Dr. Yi-De Chuang
Advanced Light Source, Lawrence Berkeley National Laboratory, Berkeley, CA 94720 USA

Prof. A. Fujimori

Department of Applied Physics, Waseda University, Okubo, Shinjuku, Tokyo 169-8555, Japan

[#] Hui Cao and Hongli Guo contributed equally to this work.

Abstract

The recent proposal of antidoping scheme breaks new ground in conceiving conversely functional materials and devices, yet the few available examples belong to the correlated electron systems. Here we demonstrate both theoretically and experimentally that the main group oxide $BaBiO_3$ is a model system for antidoping using oxygen vacancies. The first-principles calculations show that the band gap systematically increases due to the strongly enhanced Bi-O breathing distortions away from the vacancies and the annihilation of Bi 6*s*/O 2*p* hybridized conduction bands near the vacancies. Our further spectroscopic experiments confirm that the band gap increases systematically with electron doping, with a maximal gap enhancement of ~75% when the film's stoichiometry is reduced to $BaBiO_{2.75}$. These results unambiguously demonstrate the remarkable antidoping effect in a material without strong electron correlations and underscores the importance of bond disproportionation in realizing such an effect.

Keywords: Antidoping, band gap, $BaBiO_3$, breathing distortion, main group oxides, oxygen vacancies

Main Text

Introduction

In conventional semiconductors or insulators without strong electron correlations, the electron doping can be understood as extra electrons being injected either into the impurity donor band confined within the band gap (i.e. light doping), or into the conduction band (i.e. heavy doping).[1–3] The band gap either effectively decreases to be between the donor band and the conduction band or collapses, both leading to the conductivity enhancement. Recently, it is realized that an "antidoping" effect can occur[4] in a group of materials containing intermediate bands with trapped holes (electrons). In those materials, the doped electrons (holes) cause the intermediate band merge into valence band (conduction band), leading to an increase in band gap and a decrease in conductivity. This opposite doping effect opens up new perspectives in devices applications, such as battery cells, memory devices, electric sensors, etc. So far, signatures of antidoping have been observed in negative charge-transfer oxides[5–12] with strong electron correlations, such as oxygen vacancy (O_v) doped $SmNiO_3$[13–16] and $NdNiO_3$[17] and H^+ doped $SrCoO_{2.5}$.[18] Unlike transition metal oxides, the large family of main group oxides exhibit negligible electron correlations as they do not have *d* electrons in the valence or conduction band. It is unclear whether a similar antidoping effect can occur in this class of materials. The investigation on this aspect could also unravel alternative mechanisms going beyond the electronic effects.

The main group oxide $BaBiO_3$ is a negative charge-transfer insulator[19–21] and thus a model system for investigating the antidoping effect.[4] Bi in $BaBiO_3$ has a formal 4+ valence (Bi^{4+}) with a $5d^{10}6s^1$ electronic configuration, and this material has drawn long-lasting interests in the hole doping sides due to the superconductivity.[22–26] On the contrary, the electron doping side has rarely been studied.[27] The stoichiometric $BaBiO_3$ is an insulator with an indirect band gap near 0.55 eV[28] and the insulation has been attributed to a strong hybridization between Bi and O orbitals and their charge and bond disproportionation.[19,21,23,29,30] Consequently, the bismuth 6*s* and oxygen 2*p* orbital both have significant contributions to the conduction band nearest the Fermi level,[20,21] which is different from pure ligand hole states discussed in previous works.[4,15,16] One advantage of using $BaBiO_3$ is that it allows for the creation of oxygen vacancies (O_vs) to realize electron doping – beneficial for revealing the evolution of band structure without complications from the dopant bands. In addition, O_vs can be driven by electric field which promises facile applications.[16]

Here we perform both theoretical calculations and comprehensive experiments to investigate possible electron antidoping effect in $BaBiO_{3-\delta}$ ($0 \leq \delta \leq 0.25$) thin films. Theoretical calculations found that the insulating gap increases with increasing O_v concentration due to the strongly enhanced Bi-O breathing distortions away from the O_vs and the annihilation of Bi 6*s*/O 2*p* hybridized conduction bands near the O_vs. $BaBiO_3$ and $BaBiO_{3-\delta}$ thin films were experimentally fabricated with δ ranging from 0 to about 0.25. The X-ray absorption spectroscopy (XAS) and X-ray emission spectroscopy (XES) experiments demonstrate that the band gap systematically increases with increasing O_v

concentrations. Furthermore, the Raman spectroscopy and superstructure-half-order X-ray diffraction (XRD) measurements reveal the overall change of lattice breathing distortions, which is consistent with the theoretical calculation. Therefore, our study demonstrates a unique mechanism for realizing electron antidoping in $BaBiO_3$, which may inspire new prospects in controlling the electronic structures of main group oxides and related materials.

Results

The density functional theory (DFT) calculations using hybrid xc-functional (HSE06) were performed to elucidate the electronic structure change from the stoichiometric $BaBiO_3$ to O_v doped $BaBiO_{3-\delta}$ (δ = 0.25, 0.125). The calculated monoclinic $BaBiO_3$ unit cell contains two non-equivalent Bi atoms labeled as Bi1 and Bi2 as shown in the left panel of Figure 1a. The optimized Bi1-O and Bi2-O bond lengths are 2.28 Å and 2.16 Å respectively, and the tilting instability is observed with a tilting angle t = 9.49°. The difference in the bond length is b = 0.12 Å, the breathing distortion magnitude of the whole system is 2.71%, which represents the breathing distortion and agrees well to previous experiments[31,32] and calculations.[33,34] When two O_vs are introduced into to the 2×2×1 supercell at various locations (Supporting Information, Figure S1) to keep the stoichiometry at $BaBiO_{2.75}$, the most stable configuration is shown in the right panel of Figure 1a. The O_v resides in between Bi3 and Bi4, while Bi1 and Bi2 are away from O_vs. The BiO_5 tetrahedrons around Bi3 and Bi4 have similar bond lengths of ~ 2.26 Å. However, an enhanced breathing distortion on the Bi1 and Bi2 sites is observed and the long and short bond lengths are 2.32 Å and 2.18 Å respectively, which leads to an

increased bond length difference *b* of 0.14 Å, but the breathing distortion magnitude of the whole system reduces to 1.55%.

Figure 1b shows the overall density of states (DOS), which demonstrates that the band gap (indirect) increases from 0.44 eV in $BaBiO_3$ to 0.76 eV in $BaBiO_{2.75}$. The calculated band structures of both compounds are shown in Supporting Information Figure S3 which clearly demonstrates the band gap enhancement. In Figures. 1c and 1d the calculated DOS of different orbitals of $BaBiO_3$ and $BaBiO_{2.75}$ are shown respectively. The difference charge density map of $BaBiO_{2.75}$ is also calculated to demonstrate the electron transfer between bismuth and oxygen (Supporting Information Figure S4). For $BaBiO_3$, the breathing distortion *b* and the tilting angel *t* are well correlated to the bonding disproportion between two Bi-O octahedra, which can be seen in the 6*s* projected DOS (pDOS) in the top panel of Figure 1c. The Bi1 6*s* orbital has more spectral weights below the Fermi level whereas Bi2 6*s* orbital has more weights above it. There exists some back transfer of 6*p* charge to compensate the 6s charge disproportionation, thus the 6*p* orbitals exhibit an opposite trend of disproportionation compared to the 6s orbitals (middle panel of Figure 1c). It results in a bond disproportionation of $Bi^{(3+x)+}$ and $Bi^{(5-x)+}$ ($0 < x < 1$) in the stoichiometric $BaBiO_3$.[34] In addition, we see the nearly identical DOS profile for Bi2 6*s* and O 2*p* orbitals in the bottom panel of Figure 1c, suggesting the strong hybridization between them. For $BaBiO_{2.75}$, the Bi1 and Bi2 ions have the stronger inequivalent projected 6*s* DOS and larger band gap than those in the stoichiometric $BaBiO_3$ (top panel in Figure 1d). It indicates that Bi1 and Bi2 are transitioned into $Bi^{5-x'}$ and $Bi^{3+x'}$ with a

much stronger bond disproportionation. As a result, the enhanced breathing distortion on the Bi1 and Bi2 sites away from O_vs is key to the enhancement of band gap. Our calculations also show that Bi3 and Bi4 ions exhibit strongly suppressed bond disproportionation (middle panel of Figure 1d). Compared to the undoped counterpart, the DOS in the 6*s* conduction band of Bi4 vanishes, along with the strongly suppressed DOS in conduction bands of the surrounding O *p* orbitals. Since the band gap measurements are usually performed at elevated temperatures and the DFT calculations describe the ground state at 0 K, we perform *ab initio* Molecular Dynamics at 300 K in order to take the electron-phonon coupling into account. The obtained energy evolutions of electronic states in Supporting Information Figure S5, which confirms the trend of band gap enhancement in $BaBiO_3$, $BaBiO_{2.875,}$ and $BaBiO_{2.75}$ at elevated temperatures. We also calculated the phonons dispersion spectra and found that the structures remain stable when O_vs are introduced (Supporting Information, Figure S6).

To experimentally test the theoretical calculation about this novel antidoping scheme, we fabricated $BaBiO_3$ and $BaBiO_{3-\delta}$ thin films using the high-pressure reflective high energy electron diffraction (RHEED) assisted pulsed laser deposition (PLD). The samples were grown and *in-situ* annealed in the PLD chamber to obtain different levels of O_v concentration. Details about the sample fabrication can be found in Supporting Information, S2. The X-ray absorption near-edge spectra (XANES) at Bi L_3-edge were utilized to quantify the valence change of Bi cation in doped $BaBiO_{3-\delta}$ thin films (hence for quantifying the oxygen stoichiometry). For 5d Bi L_3-edge, the change of XANES spectra (e.g. edge shift or whiteline peak variation) is quite subtle so the first derivative

was applied to the absorption spectra to enhance the variations. Figure 2a shows the first derivative of the XANES spectra reported in Supporting Information Figure S7(a). Each pronounced feature (or peak) in the derivative curve may be associated with a specific electronic transition. Previously in bismuth cuprates, the derivative observed peak A, B, and C have been interpreted as transitions from Bi $2p_{3/2}$ to 6*s*, 6*d* t_{2g} and 6*d* e_g orbitals, respectively.[35,36] After backgrounds of the derivative spectra are properly removed, as shown in Fig. S7(b), we obtain a nearly linear relationship between the spectra weight (integration) and the Bi valence with the help of two Bi valence standards (e.g. Bi_2O_3 and $NaBiO_3$ powders). Based on the overall charge neutrality of the doped $BaBiO_{3-\delta}$ system and the assumption of a linear relation between the oxygen stoichiometry and the integrated area, the oxygen stoichiometry of different samples can be derived and is shown to the right axis of Figure 2b, where the highest O_v concentration corresponds to the $BaBiO_{2.75}$ phase. Furthermore, we measured the in-plane and out-of-plane lattice constants of the $BaBiO_{3-\delta}$ films (Supporting Information, Figure S9(b)) and found that the obtained lattice constants agree well with bulk $BaBiO_{3-\delta}$ samples with similar δ.[37]

To probe the band structure change in the $BaBiO_3$ and $BaBiO_{3-\delta}$ films, we measured the optical conductivity $\sigma(\omega)$ of the films using spectroscopic ellipsometry. In such measurements, the absorption peak is mainly from the direct band gap absorption and the absorption edge near the zero absorption contains the indirect band gap absorption.[1] In Figure 2c, we observed a strong absorption peak near 2.1 eV in $BaBiO_{3.05}$ and $BaBiO_{2.95}$ that have high oxygen concentrations. As oxygen atoms are stripped out of the film, the absorption peak shifts to higher energies and is about 2.2 eV in $BaBiO_{2.75}$. The optical

conductivity over a large spectral range is shown in Supporting Information Figure S10(b) which indicates the change of the background signal underneath the ~ 2 eV peak is not responsible for the peak shifting. Another striking observation is that the peak height drops quickly as the amount of O_vs increases. The absorption peak near 2 eV has been attributed to the gap opening due to the bond disproportionation.[19,20,38–40] Because the ellipsometry measurements were limited on the low energy side (~ 0.7 eV), the onsets of the absorption are not observed. We compare the photon energy E(σ_0) at which the optical conductivities all have a very small value σ_0 = 23 $\Omega^{-1}cm^{-1}$ (Supporting Information, Figure S10(a)). As shown in Figure 2d, both the absorption peak position and the E(σ_0) increase with the amount of O_vs. Additionally, we measured the ellipsometry of another set of duplicated samples which gave qualitatively similar results (Supporting Information, Figure S11).

In order to quantify the band gaps of the $BaBiO_3$ and $BaBiO_{3-\delta}$ thin films, we employed the X-ray absorption (XAS) and emission spectroscopy (XES)[41] using the fluorescence yield which probe both the unoccupied and occupied DOS (sketch shown in Figure 3a). The gap measured by the XAS and XES represent the smallest gap between the conduction and valence band, which according to the theory is an indirect gap. The first derivative shown in Figure 3b enhances the shallow peak (from the film) that would otherwise be masked by much stronger features (from the substrate) further away from the Fermi level. We obtain the band gap through fitting the first-derivative of XES and XAS spectra with Gaussian functions[42–44] and the fitting errors in Figure 3b are marked as band gap errors. The band gaps measured by XAS and XES are summarized in Figure 3c.

From the fitting results, it can be seen that the band gap systematically increases from ~ 0.59 eV to ~1.04 eV when the O_v concentration is increased. The maximal determined enhancement is about 75%, well matched by the DFT prediction. Thus, the systematic band gap enhancement trend with increased O_v concentration is identified, which experimentally confirms the antidoping effect.

Furthermore, we performed Raman spectroscopy and synchrotron half-order XRD measurements to investigate the breathing distortions in $BaBiO_{3-\delta}$ ($0 \leq \delta \leq 0.25$) films, with details shown in Supporting Information, S5. The sketch of Bi-O breathing distortion is shown in Figure 4a. First, the Raman experiments qualitatively indicate the change of the breathing distortion. Previous studies have confirmed that the Raman mode at $\approx$ 570 cm^{-1} corresponds to the breathing distortion of stoichiometric $BaBiO_3$.[40,45] The current results are shown in Figure 4b, which demonstrate that the amplitude of the Raman mode at 570 cm^{-1} is weakened as δ increases which roughly points to the weakening of the breathing distortion, though more delicate consideration has been discussed in reference.[46] Furthermore, we performed the synchrotron half-order XRD intensity profile to quantitatively determine the breathing distortion and the oxygen-octahedral-rotation (OOR)[47–49] (Supporting Information, S5). The results reveal that at room temperature the oxygen octahedral rotation type of $BaBiO_3$ is $a^- a^- c^0$, consistent with the previous neutron diffraction study,[50] while the rotation type of $BaBiO_{2.75}$ is $a^- a^- c^-$. In Figure 4c, the rotations around the pseudocubic a, b, c axes with OOR angles of α, β, γ are schematically shown. The three rotation angles and the breathing distortion Δ (the percentage variation of the Bi-O bond length) are shown in Figure 4d. It is observed that

in lightly oxygen-deficient samples (small δ), the α/β is much larger than γ, consistent with the orthorhombic symmetry. While in highly deficient samples (large δ), the α/β is similar to γ which is in line with a more symmetric structure revealed by the lattice constant[37] (Supporting Information, S5). The experimentally derived breathing distortion Δ_E is compared to the theoretical Δ_T. It is obvious that both Δ_T and Δ_E are much larger in the highly oxidized samples than the poorly oxidized samples. Therefore the above experimental findings support the modulated lattice breathing distortion as the underlying reason of the antidoping effect. The following scheme can be seen from both the theory and experiments. As O_vs are introduced, the bond disproportionation is enhanced away from the O_v and become absent near the O_v. As an overall result, the breathing distortion is reduced in average. It is accompanied with the overall OOR change by about 1 to 2 degrees. The influence of the OOR to the band gap alone is secondary.[19,51]

Discussion

The antidoping effect in $BaBiO_3$ found in the current study is driven by the response of the structural instability (breathing distortion) to the O_v doping, which is indeed different from other antidoping cases that involve transition metal elements. In those cases, the electron doping is related to large Coulomb interaction and the strong electron correlation has been used to explain the observed band gap enhancement in electron doped nickelate oxides.[13–15,17] Theoretically the doping level needs to reach 1 *e* per transition metal ion in order to activate the electron correlation and enlarge the band gap.[4,16,52] While in the current study, the partially enhanced breathing distortion on the O_v-free Bi1-O and Bi2-O sites (see Figure 1) increases the gap at doping levels much less than 1 *e*/Bi. Moreover, in

previous theoretical proposals of antidoping binary oxides (MgO, ZnO, etc.), defects such as metal vacancies are prerequisites to create polaronic hole states for the electron antidoping to take place.[4] While in antidoping $BaBiO_3$, the antidoping is initiated in the undoped phase. Additionally, the $BaBiO_3$ has very strong covalent bonds between Bi and O atoms. As a result, the oxygen hole states are extended Bloch bands which are different from those in doped binary oxides.

Conclusion

In summary, we demonstrate the antidoping effect induced in a main group oxide via the strong lattice response under the O_v doping using both DFT theory calculations and comprehensive experiments. The theory calculations show that the band gap systematically increases with O_v doping due to the enhanced bond disproportionation in Bi-O bonds away from O_vs and the suppressed bond disproportionation in Bi-O bonds next to O_vs. Experimentally, the XAS and XES measurements confirm that the band gap systematically increases with O_v doping, with a maximal gap enhancement of ~75% in $BaBiO_{2.75}$. Thus the successful antidoping of $BaBiO_3$ has been demonstrated with a root mechanism associated with the strong electron-lattice interaction which is different from previous theories. The current study manifests the extraordinary electron antidoping phenomenon in a main group oxide and opens up a new avenue for tailoring their electronic properties.

The Supporting Information is available free of charge via the internet at http://pubs.acs.org.

Calculation details; sample fabrication; XRD Characterization of lattice constants; X-ray absorption and emission spectroscopy measurements; Raman spectroscopy and XRD half-order Bragg peak measurement and quantification of oxygen octahedral rotations; Supplemental table and figures

Acknowledgments

The authors acknowledge Profs. Yi Luo, Bing Wang, Donglai Feng, Xuefeng Cui and Rui Peng for helpful discussions and experiments. The work was supported by the National Key Research and Development Program of China (Grants No. 2016YFA0401004), The Startup Fund of ShanghaiTech University, National Science Foundation of China (52072244), the Fundamental Research Funds for the Central Universities of China (Nos.WK2340000088), China Postdoctoral Science Foundation (Grant No. 2017M622498 and 2018T110789), and KAKENHI from JSPS (19K03741). Calculations are performed at the Supercomputer Center of Wuhan University and Environmental Molecular Sciences Laboratory at the PNNL. This research used resources of the Advanced Photon Source (APS), a U.S. Department of Energy (DOE) Office of Science User Facility operated for the DOE Office of Science by Argonne National Laboratory under Contract No. DE-AC02-06CH11357. The synchrotron XRD and XANES measurements were carried out at Sector 33BM, 12ID-D, 12BM-B of the Advanced Photon Source and 1W1B of the Beijing Synchrotron Radiation Facility. This research used resources of the Advanced Light Source, a DOE Office of Science User Facility under contract No. DE-AC02-05CH11231. Some XAS experiments were done at BL12B-a at the National Synchrotron Radiation Laboratory.

References

(1) Sheng S., L. *Heavy Doping Effects in a Degenerate Semiconductor.*, Semiconductor Physical Electronics.; Springer: New York, 2006.

(2) Chiang, S. Y.; Pearson, G. L. Properties of Vacancy Defects in GaAs Single Crystals. *J. Appl. Phys.* **1975**, *46* (7), 2986–2991. https://doi.org/10.1063/1.321985.

(3) Berggren, K.-F.; Sernelius, B. E. Band-Gap Narrowing in Heavily Doped Many-Valley Semiconductors. *Phys. Rev. B* **1981**, *24* (4), 1971–1986. https://doi.org/10.1103/PhysRevB.24.1971.

(4) Liu, Q.; Dalpian, G. M.; Zunger, A. Antidoping in Insulators and Semiconductors Having Intermediate Bands with Trapped Carriers. *Phys. Rev. Lett.* **2019**, *122* (10), 106403. https://doi.org/10.1103/PhysRevLett.122.106403.

(5) Mizokawa, T.; Namatame, H.; Fujimori, A.; Akeyama, K.; Kondoh, H.; Kuroda, H.; Kosugi, N. Origin of the Band Gap in the Negative Charge-Transfer-Energy Compound $NaCuO_2$. *Phys. Rev. Lett.* **1991**, *67* (12), 1638–1641. https://doi.org/10.1103/PhysRevLett.67.1638.

(6) Korotin, M. A.; Anisimov, V. I.; Khomskii, D. I.; Sawatzky, G. A. CrO_2: A Self-Doped Double Exchange Ferromagnet. *Phys. Rev. Lett.* **1998**, *80* (19), 4305–4308. https://doi.org/10.1103/PhysRevLett.80.4305.

(7) Alonso, J. A.; García-Muñoz, J. L.; Fernández-Díaz, M. T.; Aranda, M. A. G.;

Martínez-Lope, M. J.; Casais, M. T. Charge Disproportionation in $RNiO_3$ Perovskites: Simultaneous Metal-Insulator and Structural Transition in $YNiO_3$. *Phys. Rev. Lett.* **1999**, *82* (19), 3871–3874. https://doi.org/10.1103/PhysRevLett.82.3871.

(8) Mizokawa, T.; Khomskii, D. I.; Sawatzky, G. A. Spin and Charge Ordering in Self-Doped Mott Insulators. *Phys. Rev. B* **2000**, *61* (17), 11263–11266. https://doi.org/10.1103/PhysRevB.61.11263.

(9) Abbate, M.; Zampieri, G.; Okamoto, J.; Fujimori, A.; Kawasaki, S.; Takano, M. X-Ray Absorption of the Negative Charge-Transfer Material $SrFe_{1-x}Co_xO_3$. *Phys. Rev. B* **2002**, *65* (16), 165120. https://doi.org/10.1103/PhysRevB.65.165120.

(10) Takubo, K.; Mizokawa, T.; Son, J.-Y.; Nambu, Y.; Nakatsuji, S.; Maeno, Y. Unusual Superexchange Pathways in an NiS_2 Triangular Lattice with Negative Charge-Transfer Energy. *Phys. Rev. Lett.* **2007**, *99* (3), 037203. https://doi.org/10.1103/PhysRevLett.99.037203.

(11) Kuneš J.; Křápek V.; Parragh, N.; Sangiovanni, G.; Toschi, A.; Kozhevnikov, A. V. Spin State of Negative Charge-Transfer Material $SrCoO_3$. *Phys. Rev. Lett.* **2012**, *109* (11), 117206. https://doi.org/10.1103/PhysRevLett.109.117206.

(12) Choudhury, D.; Rivero, P.; Meyers, D.; Liu, X.; Cao, Y.; Middey, S.; Whitaker, M. J.; Barraza-Lopez, S.; Freeland, J. W.; Greenblatt, M.; Chakhalian, J. Anomalous Charge and Negative-Charge-Transfer Insulating State in Cuprate Chain Compound $KCuO_2$. *Phys. Rev. B* **2015**, *92* (20), 201108. https://doi.org/10.1103/PhysRevB.92.201108.

(13) Shi, J.; Zhou, Y.; Ramanathan, S. Colossal Resistance Switching and Band Gap Modulation in a Perovskite Nickelate by Electron Doping. *Nat. Commun.* **2014**, *5* (1),

4860. https://doi.org/10.1038/ncomms5860.

(14) Zhou, Y.; Guan, X.; Zhou, H.; Ramadoss, K.; Adam, S.; Liu, H.; Lee, S.; Shi, J.; Tsuchiya, M.; Fong, D. D.; Ramanathan, S. Strongly Correlated Perovskite Fuel Cells. *Nature* **2016**, *534* (7606), 231–234. https://doi.org/10.1038/nature17653.

(15) Zuo, F.; Panda, P.; Kotiuga, M.; Li, J.; Kang, M.; Mazzoli, C.; Zhou, H.; Barbour, A.; Wilkins, S.; Narayanan, B.; Cherukara, M.; Zhang, Z.; Sankaranarayanan, S. K. R. S.; Comin, R.; Rabe, K. M.; Roy, K.; Ramanathan, S. Habituation Based Synaptic Plasticity and Organismic Learning in a Quantum Perovskite. *Nat. Commun.* **2017**, *8* (1), 240. https://doi.org/10.1038/s41467-017-00248-6.

(16) Kotiuga, M.; Zhang, Z.; Li, J.; Rodolakis, F.; Zhou, H.; Sutarto, R.; He, F.; Wang, Q.; Sun, Y.; Wang, Y.; Aghamiri, N. A.; Hancock, S. B.; Rokhinson, L. P.; Landau, D. P.; Abate, Y.; Freeland, J. W.; Comin, R.; Ramanathan, S.; Rabe, K. M. Carrier Localization in Perovskite Nickelates from Oxygen Vacancies. *Proc. Natl. Acad. Sci. U. S. A.* **2019**, *116* (44), 21992. https://doi.org/10.1073/pnas.1910490116.

(17) Wang, L.; Dash, S.; Chang, L.; You, L.; Feng, Y.; He, X.; Jin, K.; Zhou, Y.; Ong, H. G.; Ren, P.; Wang, S.; Chen, L.; Wang, J. Oxygen Vacancy Induced Room-Temperature Metal–Insulator Transition in Nickelate Films and Its Potential Application in Photovoltaics. *ACS Appl. Mater. Interfaces* **2016**, *8* (15), 9769–9776. https://doi.org/10.1021/acsami.6b00650.

(18) Lu, N.; Zhang, P.; Zhang, Q.; Qiao, R.; He, Q.; Li, H.-B.; Wang, Y.; Guo, J.; Zhang, D.; Duan, Z.; Li, Z.; Wang, M.; Yang, S.; Yan, M.; Arenholz, E.; Zhou, S.; Yang, W.; Gu, L.; Nan, C.-W.; Wu, J.; Tokura, Y.; Yu, P. Electric-Field Control of Tri-State Phase

Transformation with a Selective Dual-Ion Switch. *Nature* **2017**, *546* (7656), 124–128. https://doi.org/10.1038/nature22389.

(19) Foyevtsova, K.; Khazraie, A.; Elfimov, I.; Sawatzky, G. A. Hybridization Effects and Bond Disproportionation in the Bismuth Perovskites. *Phys. Rev. B* **2015**, *91* (12), 121114. https://doi.org/10.1103/PhysRevB.91.121114.

(20) Plumb, N. C.; Gawryluk, D. J.; Wang, Y.; Ristić, Z.; Park, J.; Lv, B. Q.; Wang, Z.; Matt, C. E.; Xu, N.; Shang, T.; Conder, K.; Mesot, J.; Johnston, S.; Shi, M.; Radović, M. Momentum-Resolved Electronic Structure of the High-T_c Superconductor Parent Compound $BaBiO_3$. *Phys. Rev. Lett.* **2016**, *117* (3), 037002. https://doi.org/10.1103/PhysRevLett.117.037002.

(21) Balandeh, S.; Green, R. J.; Foyevtsova, K.; Chi, S.; Foyevtsov, O.; Li, F.; Sawatzky, G. A. Experimental and Theoretical Study of the Electronic Structure of Single-Crystal $BaBiO_3$. *Phys. Rev. B* **2017**, *96* (16), 165127. https://doi.org/10.1103/PhysRevB.96.165127.

(22) Sleight, A. W.; Gillson, J. L.; Bierstedt, P. E. High-Temperature Superconductivity in the $BaPb_{1-x}Bi_xO_3$ System. *Solid State Commun.* **1993**, *88* (11), 841–842. https://doi.org/10.1016/0038-1098(93)90253-J.

(23) Mattheiss, L. F.; Hamann, D. R. Electronic Structure of $BaPb_{1-x}Bi_xO_3$. *Phys. Rev. B* **1983**, *28* (8), 4227–4241. https://doi.org/10.1103/PhysRevB.28.4227.

(24) Cava, R. J.; Batlogg, B.; Krajewski, J. J.; Farrow, R.; Rupp, L. W.; White, A. E.; Short, K.; Peck, W. F.; Kometani, T. Superconductivity near 30 K without Copper: The $Ba_{0.6}K_{0.4}BiO_3$ Perovskite. *Nature* **1988**, *332* (6167), 814–816.

https://doi.org/10.1038/332814a0.

(25) Wen, C. H. P.; Xu, H. C.; Yao, Q.; Peng, R.; Niu, X. H.; Chen, Q. Y.; Liu, Z. T.; Shen, D. W.; Song, Q.; Lou, X.; Fang, Y. F.; Liu, X. S.; Song, Y. H.; Jiao, Y. J.; Duan, T. F.; Wen, H. H.; Dudin, P.; Kotliar, G.; Yin, Z. P.; Feng, D. L. Unveiling the Superconducting Mechanism of $Ba_{0.51}K_{0.49}BiO_3$. *Phys. Rev. Lett.* **2018**, *121* (11), 117002. https://doi.org/10.1103/PhysRevLett.121.117002.

(26) Mattheiss, L. F.; Hamann, D. R. Electronic Structure of the High-T_c Superconductor $Ba_{1-x}K_xBiO_3$. *Phys. Rev. Lett.* **1988**, *60* (25), 2681–2684. https://doi.org/10.1103/PhysRevLett.60.2681.

(27) Yan, B.; Jansen, M.; Felser, C. A Large-Energy-Gap Oxide Topological Insulator Based on the Superconductor $BaBiO_3$. *Nat. Phys.* **2013**, *9* (11), 709–711. https://doi.org/10.1038/nphys2762.

(28) Hasanuzzaman, S. M.; Iwano, K.; Nasu, K. Theory for Optical Absorption, Direct and Indirect Excitons in $BaBiO_3$. *J. Phys. Soc. Jpn.* **1999**, *68* (4), 1376–1383. https://doi.org/10.1143/JPSJ.68.1376.

(29) Tajima, S.; Uchida, S.; Masaki, A.; Takagi, H.; Kitazawa, K.; Tanaka, S.; Sugai, S. Electronic States of $BaPb_{1-x}Bi_xO_3$ in the Semiconducting Phase Investigated by Optical Measurements. *Phys. Rev. B* **1987**, *35* (2), 696–703. https://doi.org/10.1103/PhysRevB.35.696.

(30) Menushenkov, A. P.; Klementev, K. V. Extended X-Ray Absorption Fine-Structure Indication of a Double-Well Potential for Oxygen Vibration in $Ba_{1-x}K_xBiO_3$. *J. Phys. Condens. Matter* **2000**, *12* (16), 3767–3786. https://doi.org/10.1088/0953-

8984/12/16/303.

(31) Cox, D. E.; Sleight, A. W. Crystal Structure of $Ba_2Bi^{3+}Bi^{5+}O_6$. *Solid State Commun.* **1976**, *19* (10), 969–973. https://doi.org/10.1016/0038-1098(76)90632-3.

(32) Sleight, A. W. Bismuthates: $BaBiO_3$ and Related Superconducting Phases. *Physica C Supercond.* **2015**, *514*, 152–165. https://doi.org/10.1016/j.physc.2015.02.012.

(33) Franchini, C.; Kresse, G.; Podloucky, R. Polaronic Hole Trapping in Doped $BaBiO_3$. *Phys. Rev. Lett.* **2009**, *102* (25), 256402. https://doi.org/10.1103/PhysRevLett.102.256402.

(34) Franchini, C.; Sanna, A.; Marsman, M.; Kresse, G. Structural, Vibrational, and Quasiparticle Properties of the Peierls Semiconductor $BaBiO_3$: A Hybrid Functional and Self-Consistent GW+ vertex-Corrections Study. *Phys. Rev. B* **2010**, *81* (8), 085213. https://doi.org/10.1103/PhysRevB.81.085213.

(35) Retoux, R.; Studer, F.; Michel, C.; Raveau, B.; Fontaine, A.; Dartyge, E. Valence State for Bismuth in the Superconducting Bismuth Cuprates. *Phys. Rev. B* **1990**, *41* (1), 193–199. https://doi.org/10.1103/PhysRevB.41.193.

(36) Liang, G.; Sahiner, A.; Croft, M.; Xu, W.; Xiang, X.-D.; Badresingh, D.; Li, W.; Chen, J.; Peng, J.; Zettl, A.; Lu, F. X-Ray-Absorption near-Edge Structure Study of $IBi_2Sr_2CaCu_2O_y$. *Phys. Rev. B* **1993**, *47* (2), 1029–1035. https://doi.org/10.1103/PhysRevB.47.1029.

(37) Kambe, S.; Shime, I.; Ohshima, S.; Okuyama, K.; Sakamoto, K. Crystal Structure and Electronic Properties of $BaBiO_y$ ($2.5 \leq y \leq 2.9$) and $Ba_{1-x}La_xBiO_3$ ($0 \leq x \leq 0.5$). *Solid State Ion.* **1998**, *108* (1), 307–313. https://doi.org/10.1016/S0167-2738(98)00055-1.

(38) Tajima, S.; Uchida, S.; Masaki, A.; Takagi, H.; Kitazawa, K.; Tanaka, S.; Katsui, A. Optical Study of the Metal-Semiconductor Transition in $BaPb_{1-x}Bi_xO_3$. *Phys. Rev. B* **1985**, *32* (10), 6302–6311. https://doi.org/10.1103/PhysRevB.32.6302.

(39) Sato, H.; Tajima, S.; Takagi, H.; Uchida, S. Optical Study of the Metal-Insulator Transition on $Ba_{1-x}K_xBiO_3$ Thin Films. *Nature* **1989**, *338* (6212), 241–243. https://doi.org/10.1038/338241a0.

(40) Kim, G.; Neumann, M.; Kim, M.; Le, M. D.; Kang, T. D.; Noh, T. W. Suppression of Three-Dimensional Charge Density Wave Ordering via Thickness Control. *Phys. Rev. Lett.* **2015**, *115* (22), 226402. https://doi.org/10.1103/PhysRevLett.115.226402.

(41) Groot, F. de; Kotani, A. *Core Level Spectroscopy of Solids*; CRC Press, 2008.

(42) Wang, W.-C.; Chen, S.-Y.; Glans, P.-A.; Guo, J.; Chen, R.-J.; Fong, K.-W.; Chen, C.-L.; Gloter, A.; Chang, C.-L.; Chan, T.-S.; Chen, J.-M.; Lee, J.-F.; Dong, C.-L. Towards Understanding the Electronic Structure of Fe-Doped CeO_2 Nanoparticles with X-Ray Spectroscopy. *Phys. Chem. Chem. Phys.* **2013**, *15* (35), 14701–14707. https://doi.org/10.1039/C3CP52054D.

(43) Gilbert, B.; Frandsen, C.; Maxey, E. R.; Sherman, D. M. Band-Gap Measurements of Bulk and Nanoscale Hematite by Soft X-Ray Spectroscopy. *Phys. Rev. B* **2009**, *79* (3), 035108. https://doi.org/10.1103/PhysRevB.79.035108.

(44) Jovic, V.; Laverock, J.; Rettie, A. J. E.; Zhou, J.-S.; Mullins, C. B.; Singh, V. R.; Lamoureux, B.; Wilson, D.; Su, T.-Y.; Jovic, B.; Bluhm, H.; Söhnel, T.; Smith, K. E. Soft X-Ray Spectroscopic Studies of the Electronic Structure of M:$BiVO_4$ (M = Mo, W) Single Crystals. *J. Mater. Chem. A* **2015**, *3* (47), 23743–23753.

https://doi.org/10.1039/C5TA07898A.

(45) Tajima, S.; Yoshida, M.; Koshizuka, N.; Sato, H.; Uchida, S. Raman-Scattering Study of the Metal-Insulator Transition in $Ba_{1-x}K_xBiO_3$. *Phys. Rev. B* **1992**, *46* (2), 1232–1235. https://doi.org/10.1103/PhysRevB.46.1232.

(46) Menushenkov, A. P.; Troyan, I. A.; Eremets, M. I. Resonant Raman Scattering in Superconducting $Ba_{1-x}K_xBiO_3$. *J. Exp. Theor. Phys.* **2003**, *77* (9), 521–525. https://doi.org/10.1134/1.1591983.

(47) May, S. J.; Kim, J.-W.; Rondinelli, J. M.; Karapetrova, E.; Spaldin, N. A.; Bhattacharya, A.; Ryan, P. J. Quantifying Octahedral Rotations in Strained Perovskite Oxide Films. *Phys. Rev. B* **2010**, *82* (1), 014110. https://doi.org/10.1103/PhysRevB.82.014110.

(48) May, S. J.; Smith, C. R.; Kim, J.-W.; Karapetrova, E.; Bhattacharya, A.; Ryan, P. J. Control of Octahedral Rotations in $(LaNiO_3)_n/(SrMnO_3)_m$ Superlattices. *Phys. Rev. B* **2011**, *83* (15), 153411. https://doi.org/10.1103/PhysRevB.83.153411.

(49) Zhai, X.; Cheng, L.; Liu, Y.; Schlepütz, C. M.; Dong, S.; Li, H.; Zhang, X.; Chu, S.; Zheng, L.; Zhang, J.; Zhao, A.; Hong, H.; Bhattacharya, A.; Eckstein, J. N.; Zeng, C. Correlating Interfacial Octahedral Rotations with Magnetism in $(LaMnO_{3+\delta})_N/(SrTiO_3)_N$ Superlattices. *Nat. Commun.* **2014**, *5* (1), 4283. https://doi.org/10.1038/ncomms5283.

(50) Kennedy, B. J.; Howard, C. J.; Knight, K. S.; Zhang, Z.; Zhou, Q. Structures and Phase Transitions in the Ordered Double Perovskites $Ba_2Bi^{III}Bi^{V}O_6$ and $Ba_2Bi^{III}Sb^{V}O_6$. *Acta Crystallogr., Sect. B* **2006**, *62* (4), 537–546. https://doi.org/10.1107/S0108768106018842.

(51) Inumaru, K.; Miyata, H.; Yamanaka, S. Partial Suppression of Structural Distortion in Epitaxially Grown $BaBiO_3$ Thin Films. *Phys. Rev. B* **2008**, *78* (13), 132507. https://doi.org/10.1103/PhysRevB.78.132507.

(52) Zunger, A.; Malyi, O. I. Understanding Doping of Quantum Materials. *Chem. Rev.* **2021**, *121* (5), 3031-3060. https://doi.org/10.1021/acs.chemrev.0c00608.

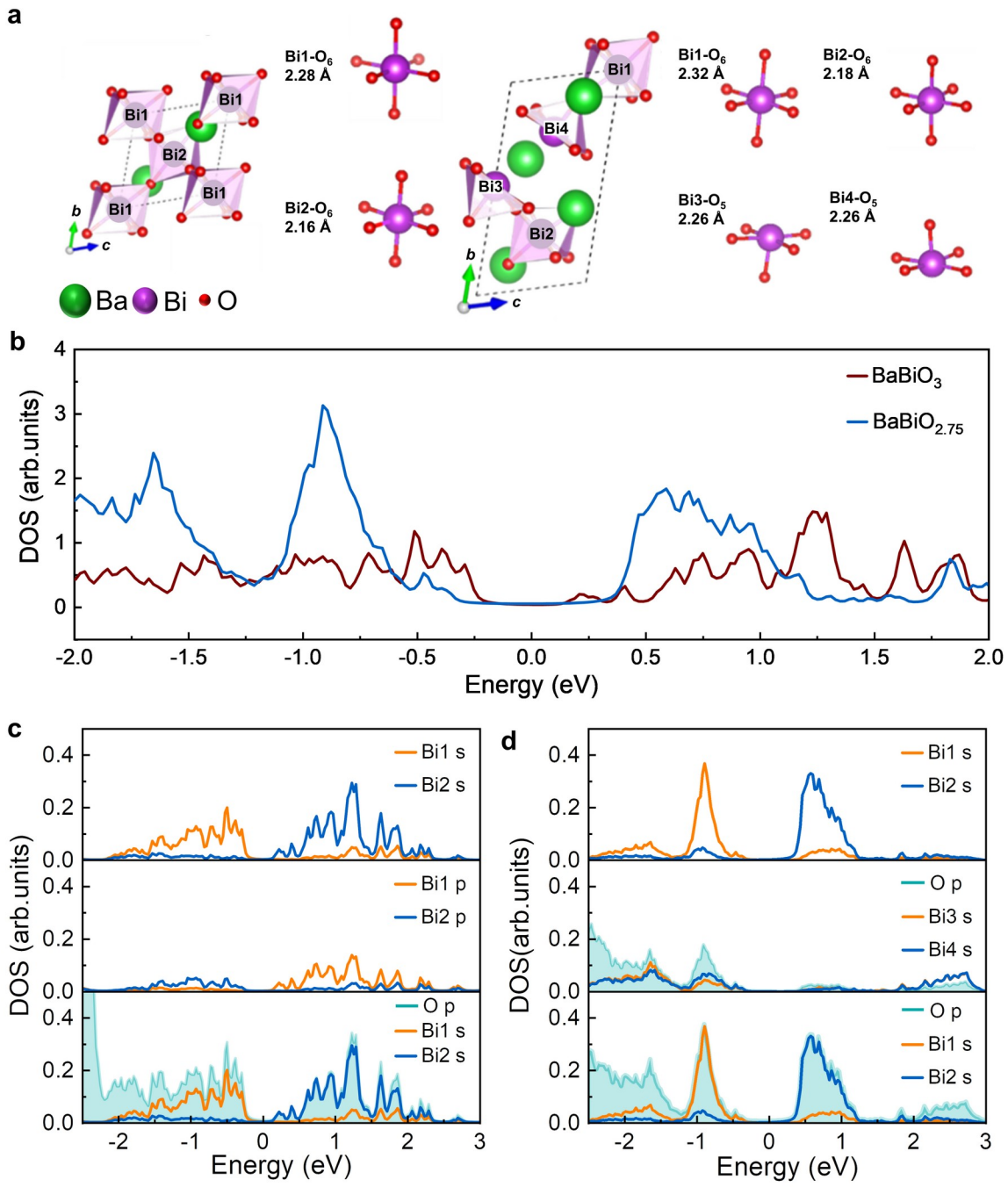

Figure 1. (a) Illustrations of atomic structures before (left) and after (right) O_v being introduced. Bi3 and Bi4 are identical to Bi1 and Bi2 before the O_v introduction. (b) The total density of states (DOS) of $BaBiO_3$ (wine) and $BaBiO_{2.75}$ (blue) showing the increased band gap with electron doping. (c) (top panel) The *s* projected DOS of Bi1 and

Bi2 ions in $BaBiO_3$, (middle panel) the *p* projected DOS of Bi1 and Bi2 ions, and (bottom panel) the overlay of Bi1/Bi2 *s* and O *p* orbitals. (d) (top panel) The *s* projected DOS of Bi1 and Bi2 in $BaBiO_{2.75}$, (middle panel) the *s* projected DOS of Bi3 and Bi4 and surrounded O *p* orbitals, and (bottom panel) the overlay of Bi1/Bi2 *s* and surrounded O *p* orbitals.

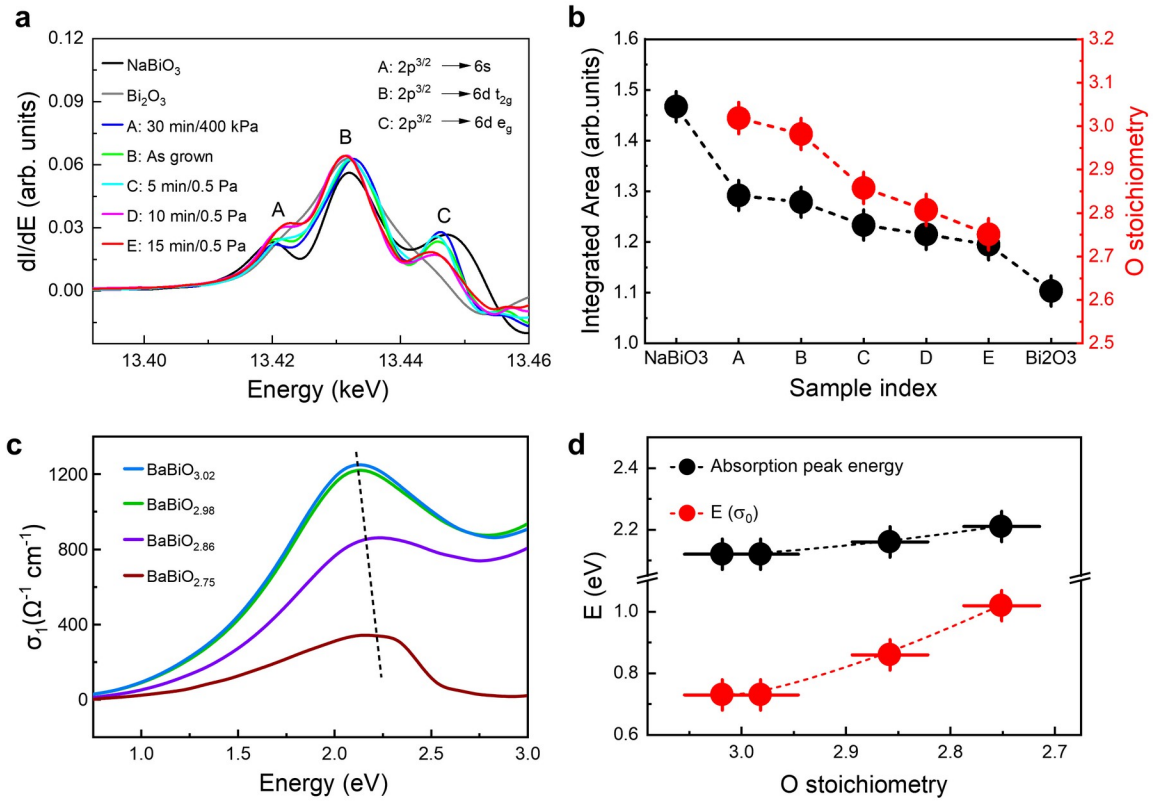

Figure 2. (a) The first derivative of Bi L_3-edge XANES spectra of the $BaBiO_{3-\delta}$ ($0 \leq \delta \leq 0.25$) films and two reference samples. (b) The correlation between the integrated area of derivative XANES spectral and the oxygen stoichiometry of $BaBiO_{3-\delta}$ ($0 \leq \delta \leq 0.25$) films and two reference samples. (c) The real part of optical conductivity σ_1 measured via spectroscopic ellipsometry. The dashed line indicates the absorption maximums. (d) The absorption peak energy and the photon energy corresponding to a small optical conductivity $\sigma_0 = 23\ \Omega^{-1}\text{cm}^{-1}$ of four films. All dashed lines are guides for eye.

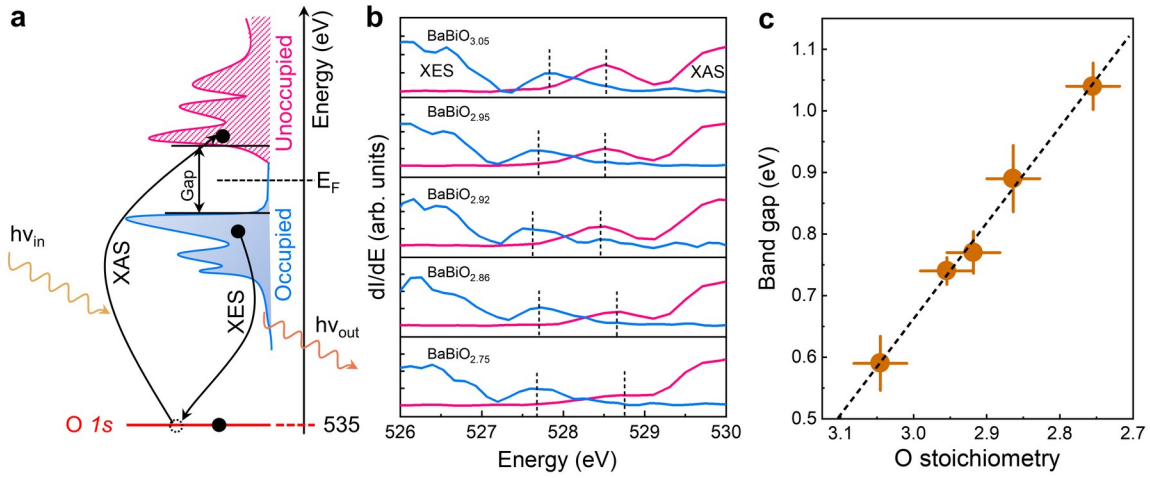

Figure 3. (a) Sketch of XAS and XES experiments; (b) The first derivative of XAS (pink) and XES (blue) spectra with determined band gap positions. (c) Band gaps of $BaBiO_{3-\delta}$ ($0 \leq \delta \leq 0.25$) thin films; the short-dashed line is a guide for eye.

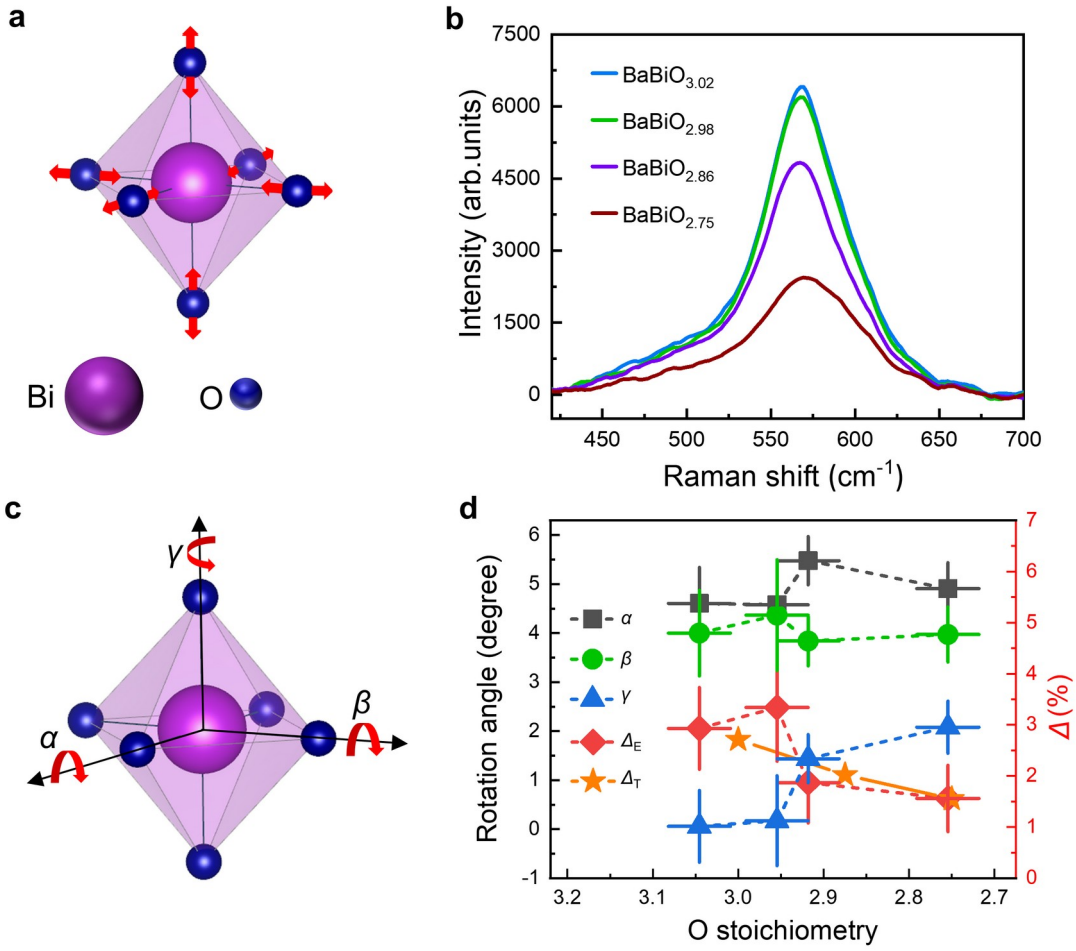

Figure 4. (a) Sketch of the Bi-O bond breathing distortion; (b) Raman spectra for $BaBiO_{3-\delta}$ films measured at 300 K under a 514 nm-Ar-laser excitation. The spectral features show a mode at ~570 cm^{-1}, which results from the oxygen breathing phonon (see Fig. 4(a)). (c) Sketch of oxygen octahedral rotation (OOR) geometry; (d) The breathing distortion amplitude measured by experiments (Δ_E) and calculated by theories (Δ_T) and OOR angles (α, β, γ) of the $BaBiO_{3-\delta}$ films.

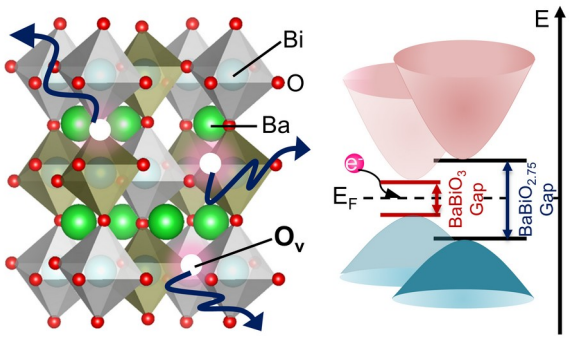

For Table of Contents Only